Editors' Suggestion | Featured in Physics

Unveiling the Superconducting Mechanism of $Ba_{0.51}K_{0.49}BiO_3$

C. H. P. Wen,[1] H. C. Xu,[1,*] Q. Yao,[1] R. Peng,[1] X. H. Niu,[1] Q. Y. Chen,[2] Z. T. Liu,[3,4] D. W. Shen,[3,4] Q. Song,[1] X. Lou,[1] Y. F. Fang,[1] X. S. Liu,[1] Y. H. Song,[1] Y. J. Jiao,[5,6] T. F. Duan,[5,6] H. H. Wen,[5,6] P. Dudin,[7] G. Kotliar,[8] Z. P. Yin,[9,†] and D. L. Feng[1,6,‡]

[1]*State Key Laboratory of Surface Physics, Department of Physics, and Laboratory of Advanced Materials, Fudan University, Shanghai 200438, People's Republic of China*

[2]*Science and Technology on Surface Physics and Chemistry Laboratory, Mianyang 621908, China*

[3]*CAS Center for Excellence in Superconducting Electronics (CENSE), Shanghai 200050, China*

[4]*State Key Laboratory of Functional Materials for Informatics, Shanghai Institute of Microsystem and Information Technology (SIMIT), Chinese Academy of Sciences, Shanghai 200050, China*

[5]*National Laboratory of Solid State Microstructures and Department of Physics, Nanjing University, Nanjing 210093, China*

[6]*Collaborative Innovation Center of Advanced Microstructures, Nanjing 210093, China*

[7]*Diamond Light Source, Harwell Science and Innovation Campus, Didcot OX11 0DE, United Kingdom*

[8]*Department of Physics, Rutgers University, Piscataway, New Jersey 08854, USA*

[9]*Department of Physics and Center for Advanced Quantum Studies, Beijing Normal University, Beijing 100875, China*

(Received 16 March 2018; revised manuscript received 8 July 2018; published 13 September 2018)

The mechanism of high superconducting transition temperatures (T_c) in bismuthates remains under debate despite more than 30 years of extensive research. Our angle-resolved photoemission spectroscopy studies on $Ba_{0.51}K_{0.49}BiO_3$ reveal an unexpectedly 34% larger bandwidth than in conventional density functional theory calculations. This can be reproduced by calculations that fully account for long-range Coulomb interactions—the first direct demonstration of bandwidth expansion due to the Fock exchange term, a long-accepted and yet uncorroborated fundamental effect in many body physics.Furthermore, we observe an isotropic superconducting gap with $2\Delta_0/k_BT_c = 3.51 \pm 0.05$, and strong electron-phonon interactions with a coupling constant $\lambda \sim 1.3 \pm 0.2$. These findings solve a long-standing mystery—$Ba_{0.51}K_{0.49}BiO_3$ is an extraordinary Bardeen-Cooper-Schrieffer superconductor, where long-range Coulomb interactions expand the bandwidth, enhance electron-phonon coupling, and generate the high T_c. Such effects will also be critical for finding new superconductors.

DOI: 10.1103/PhysRevLett.121.117002

Bismuthates were the first family of oxide high-temperature superconductors [1], exhibiting superconducting transition temperatures (T_c) up to 32 K (Refs. [2,3]). The phase diagram of bismuthate superconductors fits the paradigm of high-temperature superconductivity emerging near a competing broken-symmetry phase. $BaBiO_3$ is a perovskitelike insulator with a ~2 eV band gap [4], where a commensurate charge density wave (CDW) doubles the unit cell and is accompanied by breathing and tilting distortions of the BiO_6 octahedra [5–7]. With potassium doping, the CDW is suppressed and superconductivity develops, reaching its highest T_c of 32 K at $Ba_{1-x}K_xBiO_3$ with $x \sim 0.35$ [8]. These T_cs are much higher than those of conventional phonon-mediated superconductors with a similar density of states at the Fermi energy [8–10]. However, unlike cuprates or iron-based superconductors where superconductivity emerges near magnetic order, there is no magnetic phase anywhere in the phase diagrams of the bismuthate superconductors, suggesting a nonmagnetic pairing mechanism [8,9].

Two pictures have emerged to explain the bismuthates' long-debated pairing mechanism. One, rooted in the chemistry of the compound, posits that Cooper pairs form locally. The nominal Bi^{4+} valence is not energetically favorable and charge disproportionates into Bi^{3+} and Bi^{5+} [11,12], although the actual charge difference is much smaller than assumed in an ionic picture [13,14]. Electron pairs preferentially occupying one sublattice could give rise to the insulating CDW state. Upon increasing doping, the charge disproportionation weakens and eventually disappears, but the electron pairs may survive and Bose condense, leading to superconductivity [12,15]. It has also been stressed that one should think of these as negative charge-transfer materials, in which the holes introduced upon doping reside mainly in oxygen states of A_{1g} symmetry around the Bi sites [6,16,17].

An alternative picture posits that the pairing in the bismuthates is due to strong electron-phonon coupling, with a model of electrons coupled to optical phonons introduced for $BaPb_xBi_{1-x}O_3$ [18]. Early density functional

theory (DFT) calculations, however, found an electron-phonon coupling constant λ of 0.34, far too small to account for the high T_c [19]. More recently, it has been argued that the *long range* Coulomb interactions were underestimated in bismuthates, since they are nearly insulators and the screening should be weak. Consequently, the electron-phonon coupling is underestimated by DFT coupled with semilocal exchange-correlation functionals such as local density approximation (LDA) and generalized gradient approximation (GGA) [20]. When long range Coulomb interaction exchange terms are considered using the screened hybrid functionals and the *GW* method, the calculated bandwidth is significantly broadened, and electron-phonon coupling is increased substantially to $\lambda \simeq 1$, which could account for the high T_c of ~30 K [20]. However, as a fundamental effect that has been elaborated in many textbooks [21], the band expansion effect of long range Coulomb interaction has never been directly corroborated in any real material, and whether it could enhance the electron-phonon coupling and superconducting pairing has not been verified experimentally. Therefore, so far, long range Coulomb interaction has not been adopted as a routine process of predicting new superconductors.

To clarify the superconducting mechanism of this important superconductor family, it is crucial to obtain a comprehensive understanding of its electronic band structure and superconducting gap structure, which remain unknown. Angle-resolved photoemission spectroscopy (ARPES) is the most direct probe of electronic structure in momentum space. However, there is no ARPES report on bismuthate superconductors so far, mainly because of the poor crystal quality, three dimensional crystal structure [Fig. 1(a)], and rough surfaces from cleavages [Fig. 1(b)]. In this study, by overcoming the above issues, we have successfully obtained the electronic structure of $Ba_{0.51}K_{0.49}BiO_3$, extracted the information of long-range Coulomb interaction and electron-phonon coupling, and solved the long-standing problem of superconducting mechanism in bismuthates.

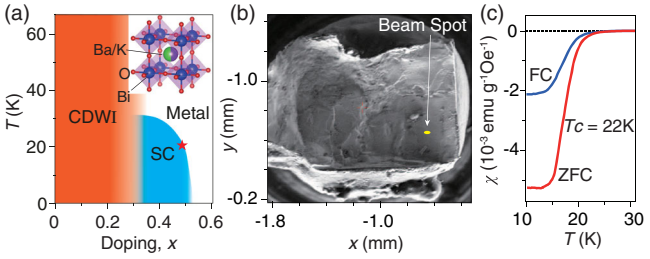

FIG. 1. (a) Phase diagram of $Ba_{1-x}K_xBiO_3$ according to [6,22]. The abbreviations stand for charge density wave insulator (CDWI) and superconductor (SC). The red marker shows the doping and T_c of our samples. The inset illustrates the perovskite-like crystal structure. (b) Scanning electron microscope image of the cleaved surface. A beam spot of 50 μm × 25 μm is illustrated. (c) Temperature dependence of the zero field-cooled (ZFC) and field-cooled (FC) magnetic susceptibility of our $Ba_{0.51}K_{0.49}BiO_3$ single crystal measured at 100 Oe.

High quality $Ba_{0.51}K_{0.49}BiO_3$ single crystals were synthesized by the self-flux method [23]. The chemical composition was determined by electron probe microanalysis (EPMA), and the crystal structure was verified by x-ray diffraction [24,25]. The T_c is 22 K [Fig. 1(c)], which is consistent with the reported phase diagram [Fig. 1(a)]. On the rough surfaces from *in situ* cleavages, 50–100 μm-size flat domains were found occasionally, on which ARPES measurements were conducted with the help of beams with small spot size (Supplemental Material Fig. S2 [24]), which is vital to adequate momentum resolution for quantitative analysis. The ARPES data were collected at the Shanghai Synchrotron Radiation Facility beam line 09U (Fig. 2, energy resolution 18 meV, beam spot size 100 μm × 50 μm), the Diamond Light Source beam line I05 (Fig. 3, energy resolution 4 meV, beam spot 50 μm × 50 μm), and the Advanced Light Source (ALS) beam line 4.0.3 (Fig. 4, energy resolution 12 meV,

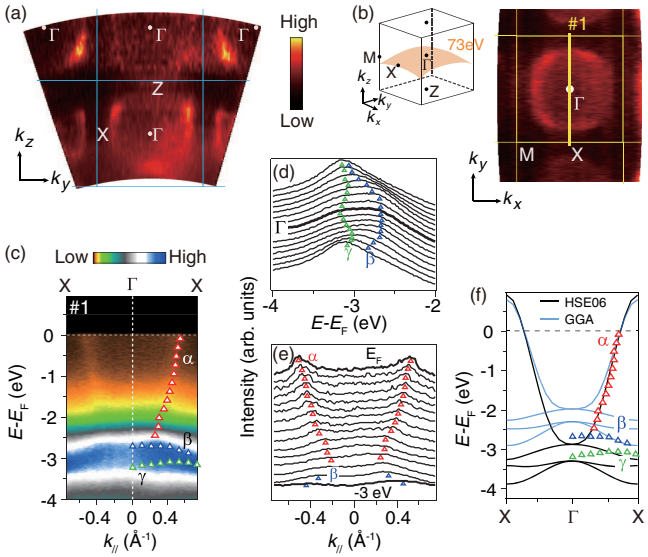

FIG. 2. (a) Photoemission intensity map in the ΓZX plane integrated over an energy window of $E_F \pm 15$ meV, measured with 57 to 132 eV photons. (b) In-plane photoemission intensity map measured with $h\nu = 73$ eV photons, integrated over $E_F \pm 15$ meV. The inset illustrates the Brillouin zone of $Ba_{0.51}K_{0.49}BiO_3$ and the momentum space sampled with $h\nu = 73$ eV photons. (c) Photoemission intensity along cut #1 in panel (b). The bands α, β, and γ are indicated on the right side by markers in red, blue, and green, respectively. (d) Energy distribution curves (EDCs) of data in the lower part of panel (c), showing the dispersions of bands β and γ. (e) Momentum distribution curves (MDCs) of data in the upper part of panel (c), showing the dispersions of bands α and β. (f) Band dispersion extracted from the photoemission data (markers in red, blue, and green) plotted over density functional theory (DFT) calculations of $BaKBi_2O_6$, using generalized gradient approximation (GGA, blue curves) and Heyd-Scuseria-Ernzerhof hybrid functional calculations (HSE06, black curves).

beam spot size 50 μm $\times$ 25 μm) under a vacuum better than 5×10^{-11} mbar.

To extract the electron-phonon coupling information from the photoemission spectra, we used the Migdal-Eliashberg formalism, where the electron-phonon spectral function, $\alpha^2F(\omega, k; \epsilon)$ is related to the imaginary part of the self-energy by $\mathrm{Im}\Sigma(\epsilon, k) = \pi \int_0^{\omega_{\max}} \alpha^2F(\omega, k; \epsilon)d\omega$ at $T \to 0$ limit. Thus, we calculate $\alpha^2F(\omega, k; \epsilon)$ by the derivative of $\mathrm{Im}\Sigma(\epsilon, k)$, where the phonon energy $\omega = E_F - \epsilon$. Then the coupling strength is calculated according to the formula $\lambda(\epsilon, k) = 2 \int_0^{\omega_{\max}} \alpha^2F(\omega, k; \epsilon)/\omega d\omega$ ([24,26]). Band structures were calculated using the VASP package [27] with GGA (in the Perdew-Burke-Ernzerhof form [28]) and HSE06 exchange-correlation functionals [29,30]. We used the simple-cubic perovskite structure with lattice constant $a = 4.27$ Å, an energy cutoff of 500 eV and a $20 \times 20 \times 20$ k mesh in both DFT-GGA and DFT-HSE06 calculations.

The three-dimensional Fermi surface structure is revealed by the combination of k_z dependent and in-plane photoemission intensity maps at the Fermi energy [Figs. 2(a)–2(b)]. The Fermi surface cross sections in the ΓZX plane match the period of the Brillouin zones when assuming an inner potential of 7 eV [Fig. 2(a)], and they match the cross section in the ΓMX plane [Fig. 2(b)] as expected. The Fermi surface is a rounded cube shape centered at Γ, consistent with theoretical calculations [19,31,32]. Based on the Fermi surface volume and Luttinger's theorem [33], the electron carrier density is estimated to be 0.48 ± 0.05 e^-/unit cell. The photoemission intensity along Γ–X shows three bands near the Fermi energy [Fig. 2(c)]. The energy distribution curves [EDCs, Fig. 2(d)] show two flat bands (β and γ) around 3 eV below the Fermi energy, while the momentum distribution curves (MDCs) show an electronlike band (α) crossing the Fermi level [Fig. 2(e)] to form the electronlike Fermi surface [Figs. 2(a)–2(b)].

At Γ, α and β are degenerate, as shown by the calculations [Fig. 2(f)]. The measured occupied bandwidth of α is unexpectedly ~34% larger than that calculated using GGA, in stark contrast to the cuprate and iron-based superconductors, where the electronic bands are strongly renormalized to be much *narrower* than the DFT-LDA and GGA bandwidth, due to short-range Coulomb interactions. Our findings indicate that the short-range Coulomb interaction strength is very weak in $Ba_{0.51}K_{0.49}BiO_3$, fundamentally different from that in cuprate and iron-based superconductors. On the other hand, the highly-dispersive α band is reproduced excellently by DFT-HSE06 [Fig. 2(f)] and the *GW* method [24,27], without any tuning parameter. A slight discrepancy near the α band bottom leads to a ~8% narrower occupied bandwidth than in the HSE06 calculation, perhaps arising from uncertainty due to broad photoemission features, or finite but weak short-range Coulomb interactions. The HSE06 hybrid functional includes the long-range exchange interaction, which results from long range Coulomb interaction and is largely omitted in the semilocal LDA and GGA functionals. This exchange interaction tends to delocalize conduction electrons and increase their kinetic energy and bandwidth [21]. Long range Coulomb interaction often plays an important role in systems with low carrier density or poor screening, such as Mott insulators [34], semiconductors [35], and semimetals [36], and the near-perfect reproduction of the observed bandwidth by HSE06 here indicates that it plays an important role in the bismuthate superconductors, likely because bismuthates are near an insulating phase. As discussed later, this interaction not only expands the electronic bands, but it also has a profound impact on the lattice dynamics and electron-phonon interactions.

The temperature dependence of the superconducting gap is investigated at the Fermi momentum (k_F) along ΓX in the ΓMX plane using 30 eV photons [Fig. 3(a)]. At 10 K, the symmetrized photoemission intensity is suppressed at E_F, indicating the opening of an energy gap. Upon increasing

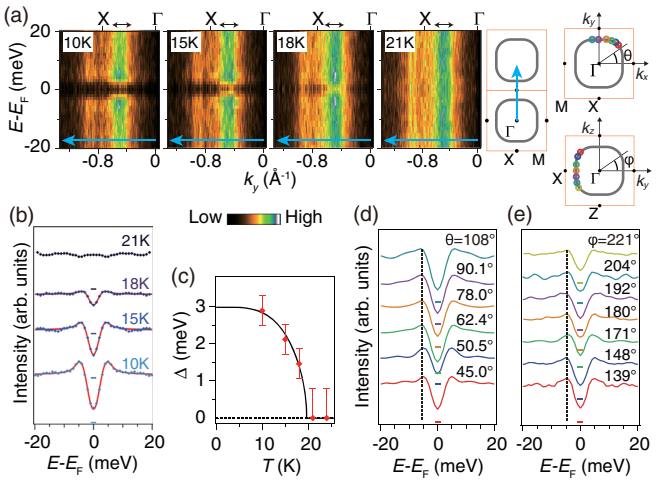

FIG. 3. (a) Temperature dependence of symmetrized photoemission spectra along the ΓX direction as shown by the photoemission cut in the right inset (blue arrow), measured in the ΓMX plane by 30 eV photons. The right insets illustrate the Brillouin zones (orange squares) and Fermi surfaces (gray). (b) Temperature dependence of the symmetrized EDCs (diamonds) integrated around k_F [double arrows above (a)]. The EDCs are vertically offset for better visualization, with horizontal bars indicating their zero positions. The red solid curves are fits to resolution-convolved Dynes functions. (c) Temperature dependence of the superconducting gap (red) fit to the BCS function (black). The error bars are determined by combining the standard deviations of the Dynes fits (c) and the energy uncertainty. (d) Symmetrized EDCs at various k_Fs (as shown in the right top inset of panel a) of band α in the ΓMX plane measured at 10 K. The EDCs are vertically offset, with horizontal bars indicating their zero positions. The top panel illustrates the Brillouin zone (orange square), Fermi surface cross section (gray), and the color-coded Fermi momenta (open circles). (e) Same as panel d but along k_Fs in the ΓZX plane [right bottom inset of panel (a)].

temperature, the gap gradually decreases and finally closes at 21 K, consistent with the T_c measured by magnetic susceptibility [Fig. 1(c)]. Below T_c, the symmetrized EDCs integrated around k_F show a superconducting gap with a coherence peak [Fig. 3(b)]. We fit the EDCs to the Dynes function [37], $N(E,\Gamma) = |\mathrm{Re}[(E-i\Gamma)/\sqrt{(E-i\Gamma)^2-\Delta^2}]|$, where $N(E,\Gamma)$ is the measured spectrum, Δ is the gap, and Γ is a broadening term (also called the scattering rate). After convolving the energy resolution, we get $\Delta(10\ \mathrm{K}) = 2.9$ meV and $\Gamma(10\ \mathrm{K}) = 0.04$ meV. Upon increasing temperature, the coherence peak intensity decreases and the gap closes. The temperature dependence of the gap fits well to the Bardeen-Cooper-Schrieffer (BCS) formula, giving a $2\Delta(0)/k_B T_c$ of 3.51 ± 0.05, consistent with previous reports on overdoped samples [38]. The superconducting gap structure in momentum space, which reflects the pairing symmetry, was investigated along the Fermi surface cross sections in the high-symmetry ΓMX and ΓZX planes (Figs. 3(d) and 3(e)]. As shown by the dashed lines tracking the coherence peaks, the gap remains constant within our uncertainty, indicating an isotropic gap.

Upon closer inspection of the ARPES spectra near k_F, a kink in the dispersion can be observed around a binding energy of 50 meV [Fig. 4(a)], which is the signature of electron-boson interactions [26]. In the dispersion extracted from the Lorentz fitting on the MDCs [Fig. 4(b)], the slope between $E_F - 50$ meV and E_F gives the Fermi velocity, v_F, and the slope on a larger energy scale approximates the bare-band Fermi velocity, v_F^0. Their difference indicates a strongly enhanced band mass. The difference between the low energy dispersion and the polynomial fit of the bare band gives the real part of the self-energy, ReΣ [Fig. 4(c)], which shows a maximum around 50 meV. The full-width at half-maximum (FWHM) of the MDCs also exhibits a prominent increase around 50 meV {Fig. 4(d) and Supplemental Material Fig. S4 [24]}, indicating a major change in the quasiparticle lifetime. The quasiparticle lifetime at E_F is not infinite as expected for an ideal Fermi liquid, because of extrinsic momentum broadening contributed by impurity scattering and local roughness on the surface (Supplemental Material Fig. S2 [24]). To exclude this, we subtract the minimum value of the FWHM around E_F as a constant background; then the FWHM is multiplied by $v_F^0/2$ to obtain the imaginary part of the self-energy, ImΣ. The ReΣ from the Kramers-Kronig transformation of ImΣ matches closely to that obtained from the dispersion [Fig. 4(c)], indicating that ReΣ and ImΣ are self-consistent. The kink and the abrupt change of ImΣ within $[-35\ \mathrm{meV}, -70\ \mathrm{meV}]$ demonstrate strong interactions between electrons and bosonic modes. Its energy coincides with an oxygen-breathing mode found around 60 meV by neutron scattering [Fig. 4(e)] [39], which is predicted to couple with electrons most strongly [20]. Therefore, the observed self-energy behavior is most likely due to the strong coupling of the conduction band to the oxygen-breathing phonon.

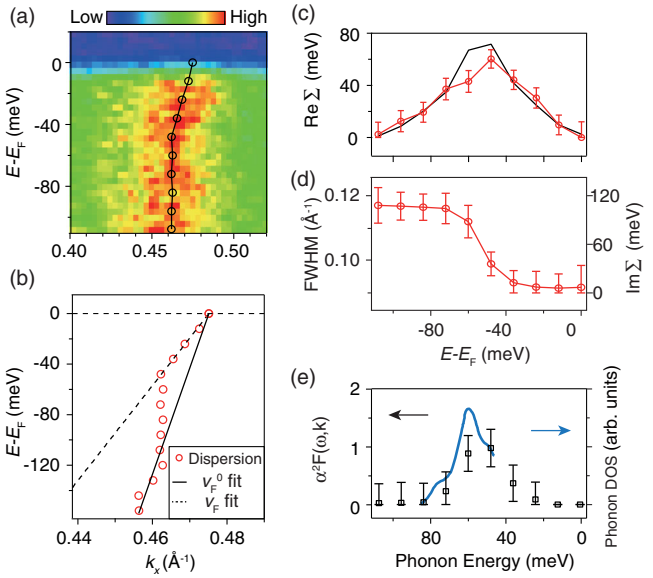

FIG. 4. (a) ARPES spectrum overlaid with the Lorentz fitting on the MDCs taken along ΓX using 72 eV photons. (b) MDC-derived dispersion from the raw data (circles), linear fits to the high energy ($E - E_F < -80$ meV, v_F^0 fit, solid line) and low energy ($E - E_F > -50$ meV, v_F fit, dashed line) dispersions. (c) Real part of the self-energy ReΣ obtained from the difference between the band dispersion near E_F and the polynomial fit approximating the bare band dispersion (red dots), and from the Kramers-Kronig transformation of the imaginary part of the self-energy ImΣ (black curve). (d) Full-width at half-maximum (FWHM) of the MDCs, and ImΣ computed from the FWHM. (e) Electron-phonon spectral function $\alpha^2F(\omega,k)$ (black squares) calculated from the $\mathrm{Im}\Sigma(\omega)$ and the phonon density of states determined by neutron diffraction [39]. To avoid unphysical values, we set negative data points of $\alpha^2F(\omega,k)$ to zero.

The electron-phonon coupling strength, λ, is central to the controversy around the superconducting mechanism of $Ba_{1-x}K_xBiO_3$. As the band velocity is renormalized from $v_F^0 = 8.0 \pm 0.8$ eV Å to $v_F = 3.5 \pm 0.4$ eV Å [Fig. 4(b)], in a simple estimate $\lambda = v_F^0/v_F - 1 = 1.3 \pm 0.2$. Alternatively, one can compute the electron-phonon spectral function, α^2F, and λ from the self-energy. We found that α^2F is in good agreement with the phonon DOS [Fig. 4(e)], and $\lambda = 1.3 \pm 0.2$ [26]. Using the McMillan equation, $T_c = (\Theta_D/1.45)\exp\{-1.04(1+\lambda)/[\lambda - \mu^*(1+0.62\lambda)]\}$ with the Debye temperature $\Theta_D = 280$ K [10], $\lambda = 1.3$, and Coulomb pseudopotential parameter $\mu^* = 0.11$, we get $T_c = 22$ K. Thus, the large λ is sufficient to explain the high T_c of this bismuthate superconductor. Based on these analyses, and the observed self-energy behavior and isotropic gap, we conclude that $Ba_{0.51}K_{0.49}BiO_3$ is a BCS superconductor.

Revealing the electron-phonon coupling strength is essential for a quantitative understanding of both the conventional BCS superconductors [40,41], and even some unconventional superconductors where electron-phonon

coupling plays a substantial role, such as monolayer $FeSe/SrTiO_3$ [42,43]. When the electronic self-energy $\Sigma(\epsilon, k)$ is negligible, linear response calculations based on LDA and GGA can compute the electron-phonon coupling strength well. However, a large long range Coulomb interaction, as in $Ba_{0.51}K_{0.49}BiO_3$, leads to a large momentum-dependent self-energy that expands the electronic band to roughly 1.4 times the LDA and GGA value and 10% reduction in the density of states at the Fermi level. A simple estimation gives rise to an overall electron-phonon coupling strength roughly $1.4^2 \times (1 - 10\%) = 1.76$ times the LDA and GGA value. Furthermore, the long range Coulomb interaction tends to delocalize electrons and overcome the overbinding problem of LDA and GGA, which gives the correct band gap for the insulating parent compound $BaBiO_3$ and a further enhancement of the LDA and GGA electron-phonon coupling. The combined effects due to the inclusion of long range Coulomb interaction result in the average coupling strength between electrons and oxygen breathing, and stretching phonons to be ~1.0, a factor of ~3 enhancement over the LDA electron-phonon coupling strength [20]. With such a large λ, the main features of optical conductivity studies can be reproduced [44]. The agreement between this calculation and our experimental findings highlights the profound impact of the long range Coulomb interaction on electron-phonon coupling.

The observed large bandwidth, that can only be correctly reproduced by including long-range exchange interactions, constitutes the first demonstration of significant bandwidth expansion introduced by the Fock term, i.e., long range Coulomb interaction, in the Hartree-Fock treatment of a many-body system. The exchange-hole effects reduce the electronic energy unequally in momentum space and thus expand the bands, as elaborated in many textbooks, for example in Fig. 17.1 of Ashcroft & Mermin's *Solid State Physics* [21]. In real materials, there are always two opposite effects with comparative orders of magnitude—the frequency dependence of self-energy, due to short-range Coulomb interactions, narrows the bands, while the momentum dependence of self-energy, arising from long range Coulomb interaction, expands them. For metals with s and p orbitals, the bandwidth calculated by LDA and GGA is usually within 10% of the experimental value, making it difficult to separate these two effects. In $Ba_{0.51}K_{0.49}BiO_3$, the narrowing effect is small, while the expansion effect is huge, which provides a unique opportunity to uncover the long range Coulomb interaction band expansion. Our data and calculations represent the first direct demonstration of this fundamental effect.

To summarize, here we present the first comprehensive characterization of the electronic structure of a bismuthate superconductor, showing that $Ba_{0.51}K_{0.49}BiO_3$ is a benchmark BCS superconductor with an isotropic superconducting gap and $2\Delta/k_BT_c = 3.51 \pm 0.05$. The sizable electron-phonon coupling strength ($\lambda \approx 1.3$) can account for the high T_c, solving a 30-year mystery. Moreover, the remarkable agreement between our data and the screened hybrid functional calculations represents the first direct experimental proof that including long-range Coulomb interactions is crucial for compounds with low carrier density or poor screening, even if the on site Coulomb interactions are weak, so that one can overcome the overbinding problem of LDA and GGA and obtain the correct band structure and electron-phonon coupling strength. This is particularly critical for the reliable prediction of new superconductors.

We gratefully acknowledge enlightening discussions with Prof. Z.-X. Shen, Prof. C. M. Varma, Prof. G. A. Sawatzky, and Dr. D. Peets, and the experimental support of Dr. J. Denlinger, Dr. Q. Q. Ge, Dr. Y. B. Huang, Dr. Z. H. Chen, Dr. T. Kim, and Dr. Z. Sun, We thank the Diamond Light Source for time on beam line I05 under Proposal No. SI11914, the Shanghai Synchrotron Radiation Facility for access to beam line 9U, and the Advanced Light Source for access to beam line 4.0.3. Some preliminary data were taken at National Synchrotron Radiation Laboratory (NSRL, China). This work is supported by the National Key R&D Program of the MOST of China (Grants No. 2016YFA0300200, No. 2017YFA0303004, No. 2016YFA0302300, and No. 2016YFA0300400), the National Natural Science Foundation of China (Grants No. 11574337, No. 11227902, No. U1332209, No. 11704073, No. 11504342, No. 11674030, and No. 11534005), and the Fundamental Research Funds for the Central Universities (Grant No. 310421113). The calculations used high performance computing cluster of Beijing Normal University in Zhuhai.

*xuhaichao@fudan.edu.cn
†yinzhiping@bnu.edu.cn
‡dlfeng@fudan.edu.cn

[1] A. W. Sleight, J. L. Gillson, and P. E. Bierstedt, Solid State Commun. **17**, 27 (1975).
[2] L. F. Mattheiss, E. M. Gyorgy, and D. W. Johnson, Phys. Rev. B **37**, 3745 (1988).
[3] R. J. Cava, B. Batlogg, J. J. Krajewski, R. Farrow, L. W. Rupp, A. E. White, K. Short, W. F. Peck, and T. Kometani, Nature (London) **332**, 814 (1988).
[4] H. Sato, S. Tajima, H. Takagi, and S. Uchida, Nature (London) **338**, 241 (1989).
[5] S. Uchida, K. Kitazawa, and S. Tanaka, Phase Transit. **8**, 95 (1987).
[6] N. C. Plumb, D. J. Gawryluk, Y. Wang, Z. Ristic, J. Park, B. Q. Lv, Z. Wang, C. E. Matt, N. Xu, T. Shang, K. Conder, J. Mesot, S. Johnston, M. Shi, and M. Radovic, Phys. Rev. Lett. **117**, 037002 (2016).
[7] K. Foyevtsova, A. Khazraie, I. Elfimov, and G. A. Sawatzky, Phys. Rev. B **91**, 121114 (2015).
[8] A. W. Sleight, Physica (Amsterdam) **514C**, 152 (2015).

[9] B. Batlogg, R. J. Cava, L. W. Rupp, A. M. Mujsce, J. J. Krajewski, J. P. Remeika, W. F. Peck, A. S. Cooper, and G. P. Espinosa, Phys. Rev. Lett. **61**, 1670 (1988).
[10] M. F. Hundley, J. D. Thompson, and G. H. Kwei, Solid State Commun. **70**, 1155 (1989).
[11] D. E. Cox and A. W. Sleight, Solid State Commun. **19**, 969 (1976).
[12] C. M. Varma, Phys. Rev. Lett. **61**, 2713 (1988).
[13] Z. X. Shen, P. A. P. Lindberg, B. O. Wells, D. S. Dessau, A. Borg, I. Lindau, W. E. Spicer, W. P. Ellis, G. H. Kwei, K. C. Ott, J. S. Kang, and J. W. Allen, Phys. Rev. B **40**, 6912 (1989).
[14] J. T. W. de Hair and G. Blasse, Solid State Commun. **12**, 727 (1973).
[15] A. Taraphder, H. R. Krishnamurthy, R. Pandit, and T. V. Ramakrishnan, Phys. Rev. B **52**, 1368 (1995).
[16] A. Y. Ignatov, A. P. Menushenkov, and V. A. Chernov, Physica (Amsterdam) **271C**, 32 (1996).
[17] A. P. Menushenkov and K. V. Klementev, J. Phys. Condens. Matter **12**, 3767 (2000).
[18] T. M. Rice and L. Sneddon, Phys. Rev. Lett. **47**, 689 (1981).
[19] V. Meregalli and S. Y. Savrasov, Phys. Rev. B **57**, 14453 (1998).
[20] Z. P. Yin, A. Kutepov, and G. Kotliar, Phys. Rev. X **3**, 021011 (2013).
[21] N. W. Ashcroft and N. D. Mermin, *Solid State Physics* (Holt, Rinehart and Winston, New York, 1976), Chap. 17, pp. 334–337.
[22] S. Pei, J. D. Jorgensen, B. Dabrowski, D. G. Hinks, D. R. Richards, A. W. Mitchell, J. M. Newsam, S. K. Sinha, D. Vaknin, and A. J. Jacobson, Phys. Rev. B **41**, 4126 (1990).
[23] Y. Jiao, W. Cheng, Q. Deng, H. Yang, and H.-H. Wen, Physica (Amsterdam) **545C**, 43 (2018).
[24] See Supplemental Material at http://link.aps.org/supplemental/10.1103/PhysRevLett.121.117002 for detailed information on the crystal characterization, surface preparation, band structure from *GW* method, and the analysis of the electronic self-energy from the photoemission data, which includes Refs. [25–27].
[25] R. M. Fleming, P. Marsh, R. J. Cava, and J. J. Krajewski, Phys. Rev. B **38**, 7026 (1988).
[26] P. Hofmann, I. Y. Sklyadneva, E. D. L. Rienks, and E. V. Chulkov, New J. Phys. **11**, 125005 (2009).
[27] G. Kresse and J. Furthmüller, Comput. Mater. Sci. **6**, 15 (1996).
[28] J. P. Perdew, K. Burke, and M. Ernzerhof, Phys. Rev. Lett. **77**, 3865 (1996).
[29] A. V. Krukau, O. A. Vydrov, A. F. Izmaylov, and G. E. Scuseria, J. Chem. Phys. **125**, 224106 (2006).
[30] T. M. Henderson, J. Paier, and G. E. Scuseria, Phys. Status Solidi B **248**, 767 (2011).
[31] S. Sahrakorpi, B. Barbiellini, R. S. Markiewicz, S. Kaprzyk, M. Lindroos, and A. Bansil, Phys. Rev. B **61**, 7388 (2000).
[32] N. Hiraoka, T. Buslaps, V. Honkimäki, J. Ahmad, and H. Uwe, Phys. Rev. B **75**, 121101 (2007).
[33] J. M. Luttinger, Phys. Rev. **119**, 1153 (1960).
[34] R. Chitra and G. Kotliar, Phys. Rev. Lett. **84**, 3678 (2000).
[35] D. Y. Qiu, F. H. da Jornada, and S. G. Louie, Phys. Rev. B **93**, 235435 (2016).
[36] D. S. L. Abergel and T. Chakraborty, Phys. Rev. Lett. **102**, 056807 (2009).
[37] R. C. Dynes, V. Narayanamurti, and J. P. Garno, Phys. Rev. Lett. **41**, 1509 (1978).
[38] A. Chainani, T. Yokoya, T. Kiss, S. Shin, T. Nishio, and H. Uwe, Phys. Rev. B **64**, 180509 (2001).
[39] C. K. Loong, P. Vashishta, R. K. Kalia, M. H. Degani, D. L. Price, J. D. Jorgensen, D. G. Hinks, B. Dabrowski, A. W. Mitchell, D. R. Richards, and Y. Zheng, Phys. Rev. Lett. **62**, 2628 (1989).
[40] B. Cristina and Y. Tsutomu, Supercond. Sci. Technol. **14**, R115 (2001).
[41] A. P. Drozdov, M. I. Eremets, I. A. Troyan, V. Ksenofontov, and S. I. Shylin, Nature (London) **525**, 73 (2015).
[42] J. J. Lee, F. T. Schmitt, R. G. Moore, S. Johnston, Y.-T. Cui, W. Li, M. Yi, Z. K. Liu, M. Hashimoto, Y. Zhang, D. H. Lu, T. P. Devereaux, D.-H. Lee, and Z.-X. Shen, Nature (London) **515**, 245 (2014).
[43] Q. Song, T. L. Yu, X. Lou, B. P. Xie, H. C. Xu, C. H. P. Wen, Q. Yao, S. Y. Zhang, X. T. Zhu, J. D. Guo, R. Peng, and D. L. Feng, arXiv:1710.07057.
[44] R. Nourafkan, F. Marsiglio, and G. Kotliar, Phys. Rev. Lett. **109**, 017001 (2012).